# RADIOLYSIS OF WATER CONTAINING DISSOLVED NITROGEN SPECIES

Pam Yakabuskie, Jiju M. Joseph and J. Clara Wren

Department of Chemistry, the University of Western Ontario
London, Ontario, Canada N6A 5B7

**Abstract:** The effects of dissolved nitrate on the γ-radiolysis of water were studied at an absorbed dose rate of 2.1 $Gy \cdot s^{-1}$ at room temperature. Air- or argon-saturated nitrate solutions at pH 6 and 10.6 were irradiated, and the aqueous concentrations of molecular radiolysis products, $H_2$, $H_2O_2$, $NO_3^-$, and $NO_2^-$, were measured as a function of irradiation time. The experimental results were compared with computer simulations using a comprehensive radiolysis kinetic model. The radiolytic process of nitrate occurs mainly through interactions with radical species generated by water radiolysis, $\bullet e_{aq}^-$, $\bullet O_2^-$ and •OH. The kinetic analyses using smaller reactions sets indicate that measured $H_2$ and $H_2O_2$ can be used to calculate radical concentrations and provide information on the redox conditions of irradiated aqueous solutions. Model data and experimental analyses show that the presence of $10^{-3}$ M nitrate increases $[H_2O_2]$ and $[H_2]$ at the expense of the related radical species and also increases the time required to reach steady state relative to the pure water case.

**Key words:** *Water radiolysis, dissolved nitrogen species ($NO_3^-$, $NO_2^-$), aerated and argon saturated, molecular radiolysis products ($H_2$, $H_2O_2$), kinetic model analysis*

## 1. INTRODUCTION

Many of the current operational and safety issues associated with nuclear power plants concerns effects of ionizing radiation on system chemistry and materials degradation. Exposed to highly ionizing radiation, water decomposes to form a range of chemically reactive species. The decomposition of water by radiolysis generates the primary radiolysis products as follows:[1]

$$H_2O \xrightarrow{\sim\sim\sim} \bullet OH, \bullet e_{aq}^-, \bullet H, HO_2\bullet, H_2, H_2O_2, H^+ \qquad (1)$$

These radiolysis products react very quickly with each other, as well as with any additional species present in the solution. These rapid reactions lead to the generation of additional secondary radiolysis products, such as $O_2$, $\bullet O_2^-$, and $\bullet O_3^-$.

Under a constant radiation field, the decomposition reaction rates of individual species quickly catch up with the radiolysis production rates, allowing the concentrations of the radiolysis products to reach steady state. Despite the relatively low steady-state concentrations of both the highly oxidizing (•OH, $H_2O_2$, $O_2$) and highly reducing ($\bullet e_{aq}^-$, •H, $\bullet O_2^-$) species, their high chemical reactivities can effectively control the local aqueous redox condition of the water. This control over the redox state of the aqueous system strongly influences the water chemistry and corrosion kinetics in radiation-exposed systems.

Nitrogen species are present in several applications in the nuclear industry: nitric acid is used in fuel processing and waste treatment, and hydrazine and ammonia are used or considered for pH controlling agents or corrosion inhibitors in nuclear facilities. Degradation of the ion exchange resin used for heavy water purification may release nitrogen compounds into the coolant and moderator fluid. Thus, it is important to understand the interactions between dissolved nitrogen species and the radiolysis products, and to determine the resulting effect of these interactions on the overall system redox condition before the nitrogen speciation can be used as a predictive measure of the redox environment.

The focus of this research is to identify the principle set of reactions that control the nitrogen speciation and steady-state radiolysis product concentrations and determine how the initial solution redox condition alters this simplified kinetic system under controlled radiation doses at room temperature.

## 2. EXPERIMENTAL

All experimental solutions were prepared daily using water (resistivity of 18.2 Mohm·cm) purified from a NANOpure Diamond UV ultrapure water system (Barnstead International). The $NaNO_3$ used for the irradiation experiments was of A.C.S. grade (Aldrich). Experiments at pH 10.6 were performed using phosphate buffer ($10^{-3}$ mol·dm$^{-3}$) and at pH 6 without any buffer, the solution pH was measured using the pH meter (Accumet).

The de-aerated solutions were prepared by purging the bulk solution with ultra high purity argon (Praxair, impurity 0.001%) for two hours. The solution was then transferred into individual 20 mL headspace vials and sealed using aluminum crimp caps with PTFE silicone septa (Agilent Technologies) in an argon-filled glove box. The aerated sample solutions were prepared by saturating the bulk solution with high purity air (hydrocarbon free air) for two hours. Each individual vial was then pre-sealed and was saturated with the high purity air for 10 minutes. A syringe was then used to transfer the sample solution to the saturated 20 mL sample vial.

The irradiation was carried out in a $^{60}$Co gamma cell (MDS Nordion) which provided the irradiation chamber with a uniform absorption dose rate of 7.7 kGy/hr determined using Fricke Dosimetry.[2,3] Individual vials were removed from the irradiation chamber at regular time intervals to allow for gas phase and aqueous phase analysis.

For gas-phase analysis, one half of the aqueous sample solution (10 mL) was removed from the irradiated vial and transferred to a new, empty vacuum-sealed vial using a gas-tight syringe (Hamilton). The gas sample was injected into the GC system (Agilent Technologies) through a gas-tight septum. The $H_2$ concentration was determined by the TCD detector and the calibration curve was prepared by injecting certified gas mixtures with concentrations of 0.1%, 1%, 3% or 5% $H_2$ (Praxair). The detection limit for the aqueous $H_2$ concentration, [$H_2$ (aq)], was determined to be $1.0 \times 10^{-5}$ mol·dm$^{-3}$. The corresponding aqueous $H_2$ concentration was calculated from the measured gas phase concentration using the known aqueous-gas partition coefficient for $H_2$, $[C_{aq}]/[C_g] = 0.019$ at 25°C.[4]

All spectrophotometric measurements were performed using a diode array UV spectrophotometer (BioLogic Science Instruments). The concentration of hydrogen peroxide

was determined by the Ghormley tri-iodide method.[5,6] In the presence of ammonium molybdate catalyst, $I^-$ is oxidized to $I_3^-$ by $H_2O_2$. The $I_3^-$ formed has a maximum absorption at 350 nm with a molar extinction coefficient of 25500 $M^{-1}\cdot cm^{-1}$. In the case of samples containing $NO_2^-$, the $H_2O_2$ analysis was performed using the KI reagent as described in the literature.[7]

The concentration of dissolved nitrite was determined from the Griess method.[8,9] The sample is first treated with a diazotizing reagent, sulfanilamide, in an acidic medium to form the intermediate diazonium salt. The diazonium salt then reacts with the coupling reagent N-(1-Napthyl)-ethylenediamine to form the stable azo compound which has a maximum UV absorption peak at 540 nm with a molar extinction coefficient of $4.0 \times 10^4$ $M^{-1}\cdot cm^{-1}$. The concentration of nitrate was determined by reducing the nitrate to nitrite using copper-coated cadmium pellets,[9,10] and total nitrite ($NO_3^- + NO_2^-$) is determined by the above method. The initial nitrate concentration was then calculated as the difference between the observed nitrite concentration following the reduction and the nitrite concentration preceding the reduction. The detection limit for $[H_2O_2]$ and $[NO_2^-]$ was determined to be $3 \times 10^{-6}$ $mol\cdot dm^{-3}$.

## 3. RESULTS AND DISCUSSION

### 3.1 Relationship Between Molecular and Radical Products of Water Radiolysis

Detection of the radical species during irradiation in the gamma cell is practically impossible due to their low concentrations and because of the space limit imposed upon by safety regulation. During irradiation, the radical species are continuously generated. The removal of the radiation source stops all further production, and radicals decompose too rapidly for any post-irradiation analysis. However, molecular species do not decompose as fast and the post-irradiation detection of molecular species is possible. Thus, these species are the only measurable indicators of the redox condition of the system.

Previously, a simple relationship between the concentrations of molecular species $H_2$ and $H_2O_2$ and radical species •OH and $\bullet e_{aq}^-$ has been derived for pure water systems based on a water radiolysis model [11] and experimental data.[12] The kinetic analysis shows that the main production pathway for both $H_2$ and $H_2O_2$ is through primary radiolysis. The main decomposition pathway for $H_2$ is the reaction with •OH and for $H_2O_2$, reactions with $\bullet e_{aq}^-$ and •OH.

<u>For $H_2$:</u>

$$H_2O \rightarrow H_2 \quad \text{by radiolysis} \qquad G_{H2} = 0.45 \qquad (R1)$$

$$H_2 + \bullet OH \rightarrow H_2O + \bullet H \qquad k_{R2} = 4.2 \times 10^7\ M^{-1}s^{-1} \qquad (R2)$$

<u>For $H_2O_2$:</u>

$$H_2O \rightarrow H_2O_2 \quad \text{by radiolysis} \qquad G_{H2O2} = 0.7 \qquad (R3)$$

$$H_2O_2 + \bullet e_{aq}^- \rightarrow \bullet OH + OH^- \qquad k_{R4} = 1.6 \times 10^{10}\ M^{-1}s^{-1} \qquad (R4)$$

$$H_2O_2 + \bullet OH \rightarrow H_2O + HO_2\bullet \qquad k_{R5} = 2.7 \times 10^7\ M^{-1}s^{-1} \qquad (R5)$$

The radiolysis of solutions containing initially $10^{-3}$ M $NO_3^-$ generates higher $H_2$ concentrations relative to the pure water system under all conditions studied. Figure 1-a shows the $H_2$ concentration in the presence of nitrate compared to pure water under aerated condition at pH 6.

This trend can be explained by considering the interactions of radiolytically produced nitrogen species with the •OH radical that controls the $H_2$ decomposition pathway. Nitrate itself is not an effective scavenger for •OH, however, under the radiation conditions, it can be reduced to nitrite, $NO_2^-$, which is a good •OH scavenger (R6) and the level of •OH will be reduced relative to that of the pure water case (Figure 1-a). This decreases the $H_2$ decomposition by R2, so the observed $H_2$ concentrations are increased in the presence of dissolved nitrogen species, compared to pure water.

$$\bullet OH + NO_2^- \rightarrow \bullet NO_2 + OH^- \qquad k_{R6} = 5.0 \times 10^9\ M^{-1}s^{-1} \qquad (R6)$$

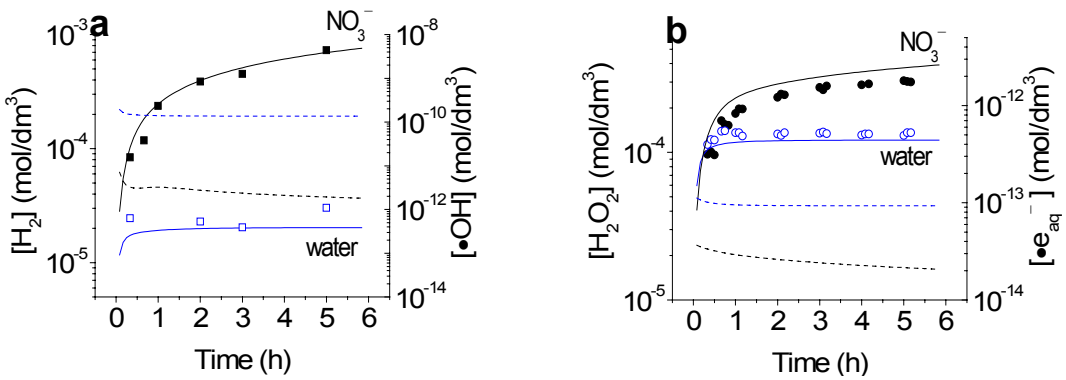


**Figure 1**: (a) $H_{2\,(aq)}$ and •OH and (b) $H_2O_2$ and $\bullet e_{aq}^-$ concentrations as a function of irradiation time under aerated conditions at pH 6. Symbols are the measured molecular concentrations, open symbols (□,○) for pure water and solid symbols (■,●) for $[NO_3^-]_0$ solutions. The solid lines (—) are the full model calculation results for the molecular species, whereas the broken lines ( – – –) are the model predicted •OH and $\bullet e_{aq}^-$ concentrations, blue lines for water and black lines for $[NO_3^-]_0$ solutions.

The $H_2O_2$ concentration is also increased in the nitrogen-containing system (Figures 1-b). This trend can be explained by considering the reactions between nitrogen species and the $\bullet e_{aq}^-$ and •OH radicals. In nitrogen-containing systems, $\bullet e_{aq}^-$ and •OH can be removed through several additional reaction pathways. The •OH radical can be removed by R6 shown above. The $\bullet e_{aq}^-$ can be scavenged by $NO_2^-$ and $NO_3^-$. The removal of $\bullet e_{aq}^-$ and •OH reduces decomposition of $H_2O_2$ by R4 and R5, thereby leading to higher $H_2O_2$ concentrations in nitrogen radiolysis systems.

$$\bullet e_{aq}^- + NO_2^- \rightarrow NO_2^{2-} \qquad k_{R7} = 3.5 \times 10^9\ M^{-1}s^{-1} \qquad (R7)$$
$$\bullet e_{aq}^- + NO_3^- \rightarrow NO_3^{2-} \qquad k_{R8} = 9.7 \times 10^9\ M^{-1}s^{-1} \qquad (R8)$$

### 3.2 Kinetic Analysis of $H_2$

For pure water under constant radiation conditions, the concentrations of primary radiolysis products, including the molecular species, quickly reach steady state therefore the steady-state concentration of $H_2$ can be approximated.

$$[H_2]_{SS} \approx \frac{k_{R1}}{k_{R2} \cdot [\bullet OH]_{SS}} \tag{E1}$$

where $k_{R1} = C_R \cdot D_R \cdot G_{H2}$ and $D_R$ is the absorbed dose rate in units of $Gy \cdot s^{-1}$ (1 Gy = 1 $J \cdot kg^{-1}$), $G_{H2}$ is the G-value (or the primary radiolysis yield) for $H_2$ in units of number of molecules produced per 100 eV absorbed energy, and $C_R$ is the unit conversion factor so that $k_{R1}$ is expressed in units of $M \cdot s^{-1}$.

This equation states that the steady-state concentration of •OH can be determined from the observed $H_2$ steady-state concentration. However, in the presence of $10^{-3}$ M nitrate, the $H_2$ concentration does not appear to reach a steady state within 5 h of irradiation, Figure 1-a. Establishing the relationship between the $H_2$ and •OH concentrations from the non steady-state concentration data increases the complexity of the kinetic analysis since the differential rate equation must be solved analytically. Assuming that the •OH concentration does not vary significantly over the reaction time and using the Taylor expansion yields:

$$\left\{1 - \frac{[H_2]}{k_{R1} \cdot t}\right\} \approx \frac{k'}{2} \cdot t \tag{E2}$$

A plot of $\left\{1 - \frac{[H_2]}{k_{R1} \cdot t}\right\}$ versus $t$ would yield a straight line, for which the slope is defined:

$$m = \frac{k'}{2} = \frac{k_{R2} \cdot [\bullet OH]}{2} \tag{E3}$$

This relationship provides an approximate, but a simplistic, method to determine the radical concentration from an observed molecular species concentration when the molecular species is not at steady state.

The •OH concentrations obtained from the slope of the plot of $\left\{1 - \frac{[H_2]}{k_{R1} \cdot t}\right\}$ vs. $t$ using the measured $[H_2]$ under different conditions are listed in Table 1. These comparisons support that the kinetic analysis based on the assumption of a principal decomposition pathway for $H_2$ through •OH (R2) is valid, and that, even in the presence of impurities, the major $H_2$ decomposition mechanism remains the same as in pure water.

**Table 1:** •OH concentrations determined from the $H_2$ experimental data compared to full model simulation

| $10^{-3}$ M $[NO_3^-]_0$ solutions | | pH 6 | | pH 10.6 | |
|---|---|---|---|---|---|
| | | **Aerated** | **De-aerated** | **Aerated** | **De-aerated** |
| **[•OH]** | Experimental | $1.42 \times 10^{-12}$ | $4.9 \times 10^{-12}$ | $5.8 \times 10^{-13}$ | $6.3 \times 10^{-13}$ |
| | **Model Simulation** (1-5h) | **$3.2–1.9 \times 10^{-12}$** | **$4.4-2.2 \times 10^{-12}$** | **$4.7-2.3 \times 10^{-13}$** | **$6.3-2.6\times 10^{-13}$** |

### 3.3 Kinetic Analysis of $H_2O_2$

The $H_2O_2$ concentration quickly reaches a steady state in the pure water system, Figure 1-b. As a result, the steady-state approximation can be applied to $H_2O_2$ for the pure water system:

$$[H_2O_2]_{SS} \approx \frac{k_{R3}}{k_{R4} \cdot [\bullet e_{aq}^-]_{SS} + k_{R5} \cdot [\bullet OH]_{SS}} \qquad \text{(E4)}$$

where $k_{R3} = C_R \cdot D_R \cdot G_{H2O2}$ and $C_R$, $D_R$, and $G_{H2O2}$ are the unit conversion factor, radiation dose rate, and G-value for $H_2O_2$ respectively.

In the presence of $10^{-3}$ M nitrate, $[H_2O_2]$ does not reach steady state as fast as in the pure water systems. However, compared to $H_2$ (Figure 1-a), $H_2O_2$ appears to reach a steady state or pseudo steady state by 5 h irradiation (Figure 1-b). The steady-state concentrations of $H_2O_2$, calculated using the semi-analytical solution (E4) with the model calculated steady-state concentrations of •OH and $\bullet e_{aq}^-$, agree very well with the direct full model results (see Table 2). The $H_2O_2$ concentrations measured at 5 h, also listed in the table, compare very well with the full-model results. These comparisons support that the kinetic analysis based on the assumption of a principal decomposition pathway for $H_2O_2$ via reactions with •OH and $\bullet e_{aq}^-$ (R4 and R5) is valid, and that, even in the presence of impurities, the major $H_2O_2$ decomposition mechanism remains the same as in pure water.

**Table 2:** Steady-state concentration of $H_2O_2$ calculated using E4 compared to full model prediction and experimental data

| $10^{-3}$ M $[NO_3^-]_0$ solutions | $[H_2O_2]_{ss}$ | | | |
|---|---|---|---|---|
| | pH 6 | | pH 10.6 | |
| | **Aerated** | **De-aerated** | **Aerated** | **De-aerated** |
| $[H_2O_2]_{SS} \approx \frac{k_{R3}}{k_{R4} \cdot [\bullet e_{aq}^-]_{SS} + k_{R5} \cdot [\bullet OH]_{SS}}$ | $4.0 \times 10^{-4}$ | $3.0 \times 10^{-4}$ | $4.1 \times 10^{-4}$ | $4.0 \times 10^{-4}$ |
| Full Model Prediction $[H_2O_2]_{SS}$ (mol·dm$^{-3}$) | $3.7 \times 10^{-4}$ | $2.8 \times 10^{-4}$ | $3.2 \times 10^{-4}$ | $2.7 \times 10^{-4}$ |
| Experimental data | $3.1 \times 10^{-4}$ | $2.3 \times 10^{-4}$ | $2.9 \times 10^{-4}$ | $2.3 \times 10^{-4}$ |

Table 3 lists the $\bullet e_{aq}^-$ concentrations under different conditions obtained by applying E4 to the $H_2O_2$ data and using the •OH concentration obtained from the $H_2$ data (Table 1). From Table 3, the $\bullet e_{aq}^-$ concentration is nearly independent of pH in the presence of $10^{-3}$ M nitrate. On the

other hand, the •OH concentration shows a dependence on pH (Table 1), and the difference in [•OH] appears to reflect on the decomposition rate of nitrate to nitrite; the higher the •OH concentration, the smaller the $NO_2^-$ production is (data not shown). This suggests that the oxidation of $NO_2^-$ by •OH back to $NO_3^-$ is an important reaction in determining the overall decomposition of nitrate, supporting our hypothesis that nitrogen compounds react with the water radiolysis products semi-catalytically.

**Table 3:** $\bullet e_{aq}^-$ radical concentrations determined from E4 using the experimental values of $H_2O_2$ (Table 2) and •OH (Table 1), compared to model simulation

| **$10^{-3}$ M $[NO_3^-]_0$ solutions** | | **pH 6** | | **pH 10.6** | |
|---|---|---|---|---|---|
| | | **Aerated** | **De-aerated** | **Aerated** | **De-aerated** |
| **$[\bullet e_{aq}^-]$** | Experimental | $2.8 \times 10^{-14}$ | $3.3 \times 10^{-14}$ | $3.2 \times 10^{-14}$ | $4.1 \times 10^{-14}$ |
| | **Model Simulation** (1-5h) | **$2.9 – 2.1 \times 10^{-14}$** | **$4.2 – 2.9 \times 10^{-14}$** | **$2.8 - 1.9 \times 10^{-14}$** | **$3.9 - 2.3 \times 10^{-14}$** |

The observation that the nitrate decomposition kinetics does not linearly correlate with the production of $H_2$ and $H_2O_2$, but reflects those of radical concentrations, further supports that the impurities such as nitrate and nitrite affect the behaviour of molecular products $H_2$ and $H_2O_2$ via their reactions with the radical species.

## 4. CONCLUSIONS

The kinetics of nitrate radiolysis was followed by monitoring the molecular water radiolysis products, $H_2$ and $H_2O_2$, as well as $NO_2^-$ and $NO_3^-$ as a function of irradiation time. The kinetics of these molecular species observed under various conditions is best described by reactions of nitrogen species with the radicals generated under irradiation conditions.

The observed rates for the radiolytic production of $H_2$ and $H_2O_2$ were analyzed using small reaction sets (R1 and R2 for $H_2$, and R3 to R5 for $H_2O_2$). Differential equations were constructed from these simple reaction sets and were solved to yield the integrated rate equations for $H_2$ (E2) and $H_2O_2$ (E4) under the assumption that the radicals involved are at a steady-state concentration. These equations provide approximate, but simple, methods to determine the •OH and $\bullet e_{aq}^-$ concentrations from the measured $H_2$ and $H_2O_2$ concentrations. This kinetic relationship verifies that the molecular species concentrations of $H_2$ and $H_2O_2$ are controlled by the behaviour of •OH and $\bullet e_{aq}^-$. The combination of E2 and E4 suggests that the concentrations of the key redox radical species can be determined from the measurements of $H_2$ and $H_2O_2$.

## ACKNOWLEDGEMENT:

This research was funded under the Natural Science and Engineering Council of Canada (NSERC) and Atomic Energy of Canada Limited (AECL) Industrial Research Chair Agreement. The chemical analysis equipment was purchased by a grant from the Canada Foundation for Innovation. We would like to thank Dr. Joanne Ball at AECL for her helpful discussion throughout the project.

## REFERENCES

1. Pastina, B.; Isabey, J.; Hickel, B. *J. Nucl. Mater.* **1999,** *264,* 309.
2. Spinks, J.W.T.; Woods, R. J. *An Introduction to Radiation Chemistry, 3rd ed*.; Wiley-Interscience: New York, 1990
3. Upadhyay, S.N.; Ray, N.K.; Goel, H.C. *Indian J. Nucl. Med.* **2002,** *17(1),* 35.
4. Drucker, K.; Moles, E. *Z. Physik. Chem.* **1910**, *75*, 418.
5. Hochanadel, C.J. *J. Phys. Chem.* **1952,** *56,* 587.
6. Stefanic, I.; LaVerne, J.A. *J. Phys. Chem. A.* **2002,** *106,* 447.
7. Schwarz, H.A.; Salzman, A.J. Radiation Research. **1958**, *9*, 502.
8. Slack P.T. *Analytical Methods Manual, 2nd edition.* Leatherhead Food R.A.: 1987.
9. Sun J.; Zhang, X.; Broderick, M.; Fein, H. *Sensors*. **2003,** *3*, 276.
10. Cortas, N.K.; Wakid, N.W. *Clin. Chem.* **1990,** *36(8),* 1440.
11. Wren, J.C.; Ball, J.M. *Radiat. Phys. Chem.* **2001,** *60,* 577.
12. Joseph, J.M.; Choi, B.S.; Yakabuskie, P.; Wren, J.C. *J. Phys.Chem*. (submitted)